

Investigating the Optoelectronic and Thermoelectric Properties of CdTe Systems in Different Phases: A First-Principles Study

Hazem Abu-Farsakh, Banat Gul, and Muhammad Salman Khan*

Cite This: *ACS Omega* 2023, 8, 14742–14751

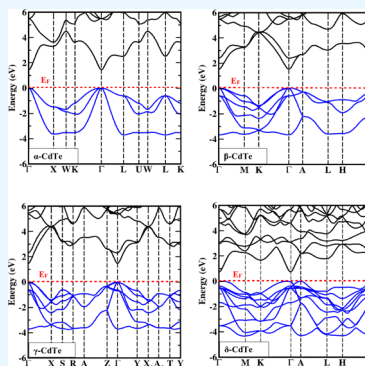
Read Online

ACCESS |

Metrics & More

Article Recommendations

ABSTRACT: CdTe is a potential material for making efficient and stable solar cells. The present study aimed to systematically investigate the electronic, optical, and thermoelectric properties of different structural phases of CdTe using density functional theory. The electronic properties were calculated using the modified Becke–Johnson potential with the local density approximation (LDA) correlation. The band structure profiles showed a direct band at the Γ -point for α -cubic, β -hexagonal, γ -orthorhombic, and an indirect band type for the δ -trigonal phase from the A-point at valence band maximum to the Γ -point at conduction band minimum. Hybridization between $Te-p$ and $Cd-s$ bands in the main valence region was observed in the partial density of states plots for all the studied phases. The real component static values of the dielectric function showed a slight decrease with increasing photonic energy after an initial small increase. The intensity of the imaginary component increased above the threshold energy for each phase, with the δ -phase showing a higher reflectivity spectrum than the other phases due to its intense peaks, making it ideal for protecting against high energy radiations. The results indicated that our computed band gaps and refractive index $n(\omega)$ were inversely related. The thermoelectric parameters calculated for these phases suggest that they have potential to be used in thermoelectric devices.



1. INTRODUCTION

Recently, group II–VI semiconducting materials and their alloys have attracted the interest of many researchers for their remarkable technological applications such as in photovoltaics,¹ in electro-optic crystals with fast response time, and in light emitting diodes.^{2–4} This inspired many researchers to model band offsets⁵ and structural and thermoelectric properties⁶ and to study various fundamental physical properties of these materials based on the first-principles calculation.^{7,8} Since they are well-tailored to the solar spectrum, the group II–VI semiconductors such as CdTe are considered to be a good choice to be used as a semiconductor in photovoltaic arrays. With a direct band gap for the hexagonal phase and cubic phase, CdTe shows a remarkable semiconducting nature with great light energy absorbing capability. CdTe also proved to offer a reputable optical response over an inclusive temperature range and provide sufficient mechanical durability as a substrate material amongst the available longer wavelength (418 nm) transparent II–VI materials.⁹ The CdTe material possesses a decent resilience to moisture sensitivity and is reasonably priced. These qualities offer the possibility of producing high-efficiency modules using inexpensive production techniques.^{10,11} One or the other of these phases can be thermodynamically more stable at 3001 K, as noted.¹² The optical characteristics of solids are a very hot topic both in basic sciences and practical applications.

The genesis of several excitation processes has fundamental importance, and their makeup employs them in a variation of optoelectronic devices. These many areas of interest demanded the integration of theory and experiment that in turn necessitates the use of reliable theoretical approaches. While most data in the literature is reported on the cubic zinc-blende phase, theoretical features of the optical characteristics of the CdTe system, notably in the other phases, have been examined very rarely. Based on the full-potential augmented-plane-wave and local orbitals technique, Merad et al.¹³ investigated the electrical and optical characteristics of the strained CdTe and ZnTe in zinc-blende phases, i.e., the d-states of the constituent metals in these materials. By using the first-principles approach within the local-density approximation, Huang and Ching¹⁴ investigated the electronic and linear optical properties of 18 cubic binary chalcogenides. Deligoz et al.'s¹⁵ ab-initio calculation was based on the density functional theory and the norm-conserving pseudopotentials exploring the electronic, elastic, and lattice dynamical features of (CdS, CdSe, and

Received: February 6, 2023

Accepted: April 4, 2023

Published: April 13, 2023



CdTe) chalcogenides. Dubowski et al.¹⁶ carried out a photoemission study of the electrical structure of Cd_{1-x}Mn_xTe (0 < x < 0.65) in the 20–140 eV photon energy range. In the cubic phase of the CdTe system, Markowski and Podgorny¹⁷ calculated the density of states and the direct interband contributions to the joint density of states by employing a self-consistent semi-relativistic type of linear muffin-tin orbital computations of the band structures. In order to interpret new ellipsometry observations, Alouani et al.¹⁸ computed the complex dielectric functions for the semiconductors such as Ge, InSb, GaAs, and CdTe. Similarly, ZnTe, CdTe, and HgTe fundamental reflectivity has been measured by Cardona and Greenaway¹⁹ spanning the energy ranges of 1.0 up to 25 eV at the ambient temperature and 1.0 up to 6.5 eV at 771 K temperature.

Some optical characteristics of CdTe samples having a carrier concentration of around 10¹⁵ cm³ have been observed by Davis and Shilliday.²⁰ Accurate first-principles studies related to the optical characteristics of several semiconductors have been a rather regular problem in recent years due to the extensive application of DFT. It is commonly accepted for genuine crystals that somewhat uneven electronic distributions are locally characterized by their density. By using this technology, the optical performance was enhanced in addition to the electronic properties. This is mostly clarified by band gap corrections, but optical absorption is also impacted by the k-dependency of the interacting energies across the band gap. Researchers are now favoring theoretical methods because experimental work requires too much effort, expensive chemicals, accurate results, and a lot of time. The most precise method to determine all the ground-state properties of different types of materials is to use DFT calculations. According to this interpretation, extremely advanced computational tools support and aid researchers in assessing physical features. Understanding the band gap and the anticipated density of states in these semiconductors is crucial. Some cutting-edge technologies from recent years totally depend on band gaps and optical absorption. In-depth research of the structural, optoelectronic, and thermoelectric characteristics of these structural phases of the binary CdTe chalcogenides is the main objective of the current study.

2. COMPUTATIONAL DETAILS

The modified Becke–Johnson potential with LDA correlation (mBJLDA) calculations for the electronic properties were performed employing the ABINIT ab-initio pseudopotential plane-waves code²¹ and using optimized norm-conserving Vanderbilt pseudopotentials.²² The crystal structures used in this study were obtained from the Materials Project database. As shown in Figure 1, the CdTe system crystallizes in the α - (cubic) (space group of *F43m*), β - (hexagonal) (space group of *P6₃mc*), γ - (orthorhombic) (space group of *Cmc21*), and δ - (trigonal) (space group of *P3121*). Optimal pseudopotentials for the Cd atoms were used.²³ The used *k*-point Brillouin zone sampling and plane-wave cutoff energies produce total energies that are converged to less than 1 meV per atom. The atomic structures were optimized employing the Perdew–Burke–Ernzerhof generalized gradient approximation (PBE–GGA) exchange and correlation functional.²⁴ The optical and thermoelectric property calculations are performed using the FP-LAPW method that works under the DFT (density functional theory) and as employed in WIEN2K²⁵ and BoltzTrap packages.²⁶ In the context of Wien2k, a full-

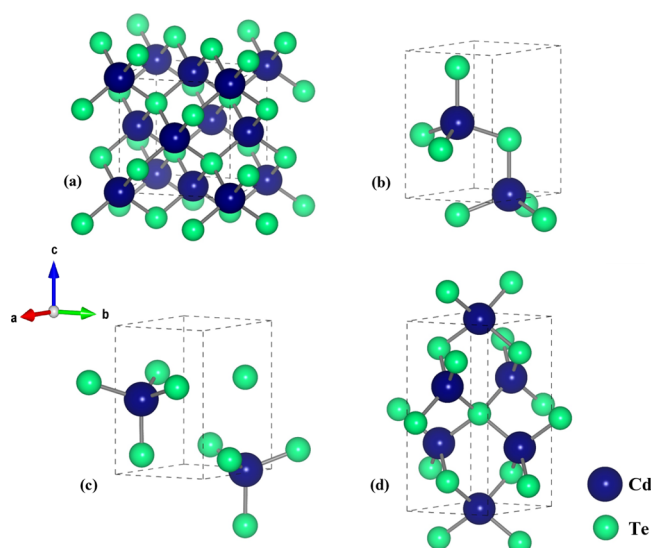


Figure 1. Computed unit cell structures for the (a) α -CdTe (cubic), (b) β -CdTe (hexagonal), (c) γ -CdTe (orthorhombic), and (d) δ -CdTe (trigonal) phases.

potential linearized augmented-plane-wave (FLAPW) code, Bethe–Salpeter equation (BSE) calculations can be performed to obtain accurate optical properties of materials. In these calculations, the ground-state electronic band structure obtained from DFT calculations serves as the input for BSE. The optical parameters of these different phases of the CdTe material were obtained from the dielectric function expressed as $\epsilon(\omega) = \epsilon_1(\omega) + i\epsilon_2(\omega)$; here, the first part represents a real and the second part represents an imaginary component of the frequency-dependent dielectric constant. The imaginary component is associated with the total absorbed energy by the material and is also related to the optical band gap of the materials.^{27,28} These real and imaginary parts are most likely given as follows:²⁹

$$\epsilon_1(\omega) = 1 + \frac{2}{\pi} \int_0^{\infty} \frac{\epsilon_2(\omega')}{\omega'} d\omega' \int_0^{\infty} \frac{1}{\omega'^2 - \omega^2} d\omega' \quad (1)$$

$$\epsilon_2(\omega) = \frac{e^2 \hbar^2}{\pi m^2 \omega^2} \sum_{v,c} \int |M_{cv}(k)|^2 \delta[\omega_{cv}(k) - \omega] d^3k \quad (2)$$

In relation 2, " \hbar " is the reduced Planck constant, " m " represents the mass of the electron, $M_{cv}(k) = u_{ck}/e\Delta/u_{vk}$ is the dipole matrix momentum of the electric field, " e " is the vector potential which shows the electric field matrix between the valence and conduction states transition, $\omega_{cv}(k) = E_{ck} - E_{vk}$ shows the transition energy, and " d^3k " is the volume element of the Brillouin zone. The other significant optical parameters like the absorption coefficient, the electron energy loss function, the refractive index, and the reflectivity were attained from $\epsilon_1(\omega)$, and $\epsilon_2(\omega)$ by means of the given equations.^{27,28}

$$I(\omega) = \frac{\sqrt{2}\omega}{c} (\sqrt{\epsilon_1^2(\omega) + \epsilon_2^2(\omega)} - \epsilon_1(\omega))^{1/2} \quad (3)$$

$$L(\omega) = \frac{\epsilon_2(\omega)}{\epsilon_1^2(\omega) + \epsilon_2^2(\omega)} \quad (4)$$

Table 1. Calculated Atomic Positions, Lattice Constants, Unit Cell Volume, Bulk Modulus (B), and Formation Energy (E_{form}) for the Studied Different Structural Phases of the CdTe System

structures										
α -CdTe		PBE		a (Å)	b (Å)	c (Å)	V_o (Å ³)	B (GPa)	E_{form}	
(F43m)		GGA							(eV/f.u.)	
				6.62	6.62	6.62	291.30	71.46	-1.37	
				6.42 ¹³						
				6.52 ¹⁴						
				6.44 ¹⁸						
				6.56 ¹⁹						
				6.48 ²⁰						
Atoms	x	y	z							
Cd	0.500	0.000	0.500							
Te	0.250	0.250	0.250							
β -CdTe										
(P6 ₃ mc)										
Cd	0.666	0.333	0.500	4.68	4.68	7.67	145.82	83.21	-1.39	
				4.57 ³⁵	4.57 ³⁵	7.47 ³⁵				
Te	0.666	0.333	0.874							
γ -CdTe										
(Cmc21)										
Cd	0.500	0.651	0.999	4.72	8.07	7.63	291.04	68.74	-1.34	
Te	0.500	0.317	0.875							
δ -CdTe										
(P3121)										
Cd	0.506	0.000	0.333	4.62	4.62	10.49	194.48	64.73	-1.33	
Te	0.502	0.000	0.833							

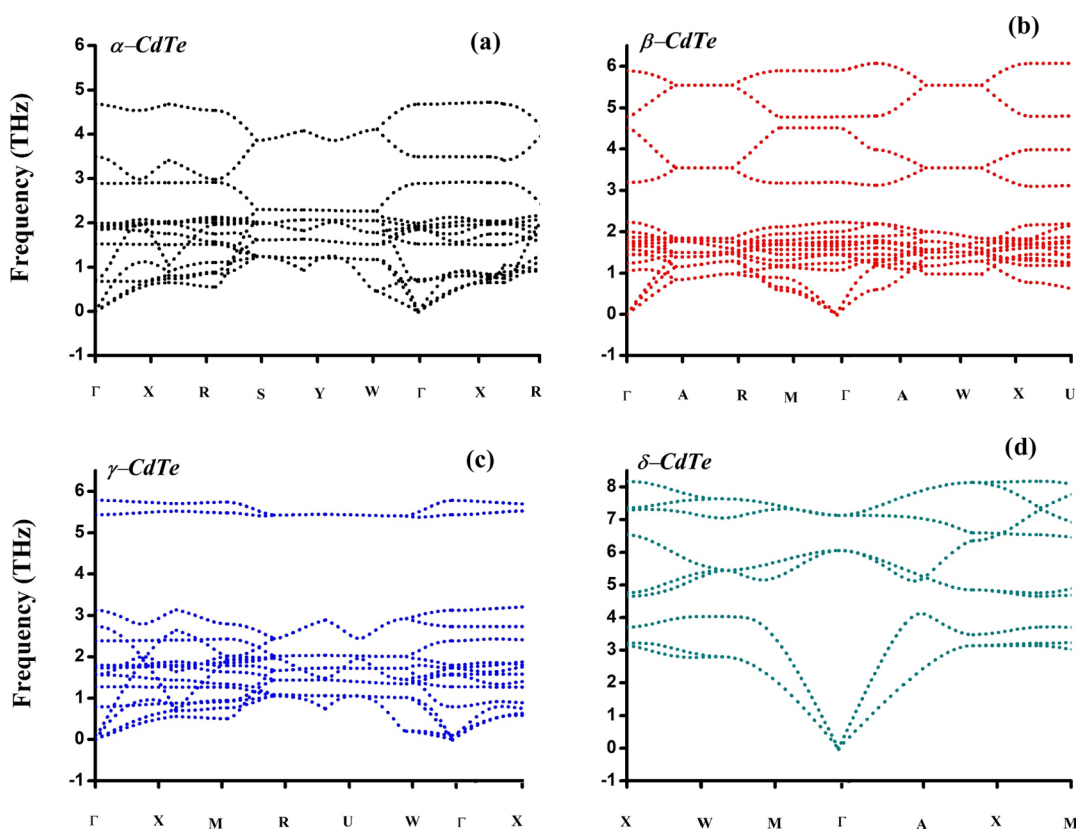


Figure 2. Calculated phonon dispersion plots for (a) α -CdTe (cubic), (b) β -CdTe (hexagonal), (c) γ -CdTe (orthorhombic), and (d) δ -CdTe (trigonal).

Table 2. Calculated Band Gaps of CdTe in Different Structural Phases

system			band gap (eV)			
		sp. group	direction		PBE–GGA	mBJLDA
α -CdTe	cubic	$F\bar{4}3m$	direct	Γ	0.58	1.45
β -CdTe	hexagonal	$P6_3mc$	direct	Γ	0.61	1.49
γ -CdTe	orthorhombic	$Cmc2\bar{1}$	direct	Γ	0.60	1.48
δ -CdTe	trigonal	$P\bar{3}121$	indirect	A \rightarrow Γ	0.01	0.75
			direct	Γ	0.05	0.77

$$n(\omega) = \left(\frac{1}{2} [\sqrt{\varepsilon_1^2(\omega) + \varepsilon_2^2(\omega)} + \varepsilon_1(\omega)] \right)^{1/2} \quad (5)$$

$$R(\omega) = \left| \frac{\sqrt{\varepsilon_1(\omega) + i\varepsilon_2(\omega)} - 1}{\sqrt{\varepsilon_1(\omega) + i\varepsilon_2(\omega)} + 1} \right|^2 \quad (6)$$

Moreover, the thermoelectric transport properties are computed with the BoltzTrap code. By means of the Boltzmann transport theory, these important thermoelectric parameters can be calculated by employing the Onsager relations.³⁰

$$\vec{J} = \sigma E_O - \sigma S \nabla T \quad (7)$$

$$\vec{J} = \sigma S T E_O - \kappa \nabla T \quad (8)$$

Here, the terms J , S , σ , E_O , and ∇T represent the electrical-current density, Seebeck coefficient, electric conductivity, external electric field, and the temperature gradient, respectively. The symbol κ here denotes the thermal conductivity, achieved from the electrical conductivity by employing the Wiedmann–Franz law.

3. RESULTS AND DISCUSSION

3.1. Electronic Properties. We computed the atomic positions, the lattice constants, and bulk modulus calculations for these structural phases. By employing the PBE–GGA, the optimized sites of each individual atom are displayed in Table 1. Similarly, to predict the thermodynamic stability, the formation energies are also computed, as listed in Table 1. Each of the studied structural phase rests considerably lower as compared to the corresponding elemental hull, with their energies between the range of -1.31 (eV/f.u.) to -3.00 (eV/f.u.). These formation energies indicate a very strong linkage with an ionic character in the Cd–Te bonds. The formation energy values for these studied phases are much consistent in terms of the convex hull that was near the composition of interest.^{37–40} Figure 2a–c shows plots of the phonon dispersions for the studied phases by employing the CASTEP package³⁷ which also works under the framework of DFT. The stable nature of these studied phases was predicted and confirmed from the phonon dispersion calculations. Our calculations clearly signify that the nonoccurrence of the negative frequencies undoubtedly confirmed that our studied structural phases of the CdTe system are dynamically stable in nature. The electronic band structures of the CdTe systems were first calculated within the PBE–GGA approach. The obtained band gaps are summarized in Table 2. The results show that the band gaps of the CdTe systems in the cubic, hexagonal, and orthorhombic phases are close in values, of 0.58, 0.61, and 0.60 eV, respectively, while for the trigonal phase, the band gap is significantly smaller and has a value of 0.01 eV. The Fermi level is arbitrarily shifted to zero.

Additionally, the band gaps are direct at the Γ -point except in the trigonal phase where the indirect band gap from the A-point at the VBM to the Γ -point at the CBM is slightly smaller than the direct band gap at the Γ -point. Since the LDA and GGA functionals are well known for their underestimation of the band gaps, and in order to obtain more accurate band gaps, we also employed the modified Becke–Johnson potential with the LDA correlation (mBJLDA)^{31,32} using pseudopotential plane waves (mBJLDA@PP). The mBJLDA@PP approach provides band gaps with an accuracy comparable to more sophisticated methods such as hybrid functionals and GW³³ at significantly lower computational costs. It is worth noting that an important drawback of the mBJLDA potential approach is that it underestimates bandwidths and overestimates carrier effective masses;²⁴ hence, we shall focus only on the obtained band gaps. The mBJLDA band gaps (shown in Table 2) are significantly larger than the PBE band gaps. The band gap of CdTe in the cubic zinc-blende structure is 1.45 eV, which is in agreement with the experimental value of 1.501 eV.³⁴ We also note that the band gaps for the cubic, hexagonal, and orthorhombic phases are close in values of 1.45, 1.49, and 1.48 eV, respectively. Additionally, the band gap is indirect for the trigonal phase and has a value of 0.75 eV.

The band structures along high symmetry lines in the Brillouin zones of the abovementioned systems are displayed in Figure 3. To gain more insight into the mBJLDA band

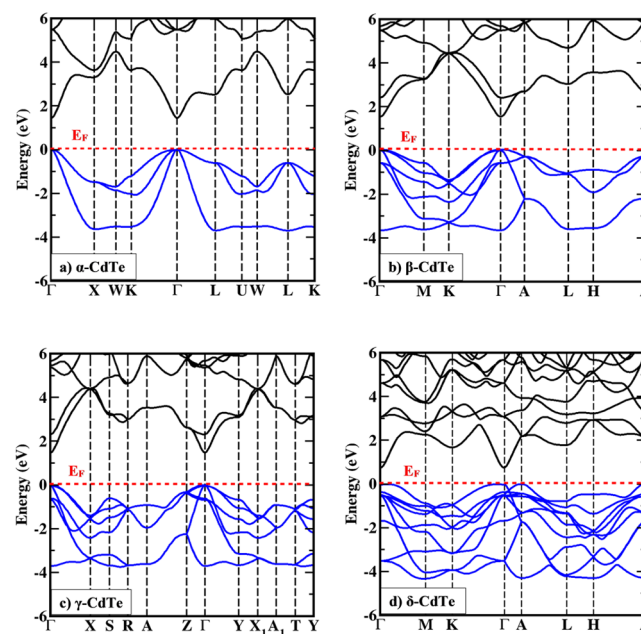


Figure 3. Electronic band structure of the different CdTe systems within the mBJLDA approach. (a) α -CdTe (cubic), (b) β -CdTe (hexagonal), (c) γ -CdTe (orthorhombic), and (d) δ -CdTe (trigonal).

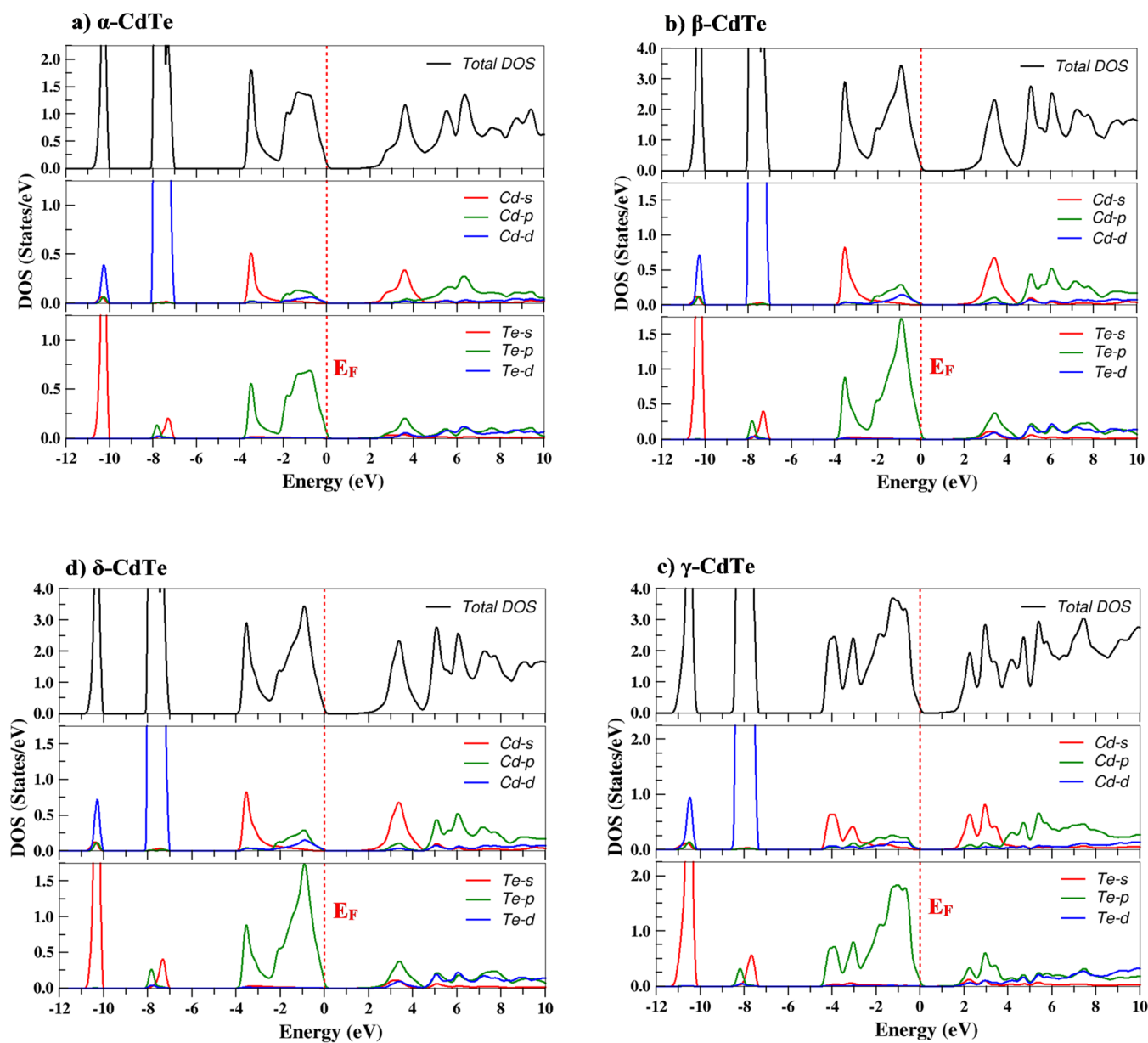


Figure 4. Computed total density of states and orbital-projected density of states for the CdTe systems obtained with the mBJLDA potential. (a) α -CdTe (cubic), (b) β -CdTe (hexagonal), (c) γ -CdTe (orthorhombic), and (d) δ -CdTe (trigonal).

structures, we presented the density of states (DOS) and the orbital-projected density of states (PDOS) for the different structures, as shown in Figure 4. The PDOS plots show that for all structures, the upper valence bands are mainly formed by the anion Te p -states, while the lower conduction band has the cation Cd s -character, with the Cd bands of the p -character appearing higher in energy in the conduction region. The semi-core Cd $4d$ -bands are located below the main valence band region (~ 7 – 8 eV below VBM), followed by the semi-core Te $5s$ -bands (~ 10 – 11 eV below VBM). It can be also noted from the PDOS plots that there is hybridization between the Te p -bands and Cd bands in the main valence region. Mainly, Cd bands of the p -character appear in the upper part of the valence bands, with a smaller contribution from the Cd bands of the d -character, followed by Cd s -character bands appearing in the lower part in the main valence bands (~ 2 – 4 eV below VBM). Lastly, it can be noted that the main valence bandwidth in the

trigonal δ -CdTe is larger than that in the other structures, which indicates less localization of the Te p -bands.

3.2. Optical Properties. The light energy that passes through materials causes a variety of phenomena that are described by a plethora of parameters that predict the optical performance of materials. The dielectric function (ω) is considered to be the most significant parameter in linear optics which explicates the absorption and polarization properties of materials. It is expressed as $\epsilon(\omega) = \epsilon_1(\omega) + i\epsilon_2(\omega)$ in which $\epsilon_1(\omega)$ is termed as the real component and $\epsilon_2(\omega)$ is the imaginary component of the complex dielectric function. To characterize the incident photon influence on the studied four phases α -CdTe, β -CdTe, γ -CdTe, and δ -CdTe materials, the dielectric function's real and imaginary components along with the other vital linear optical parameters are resolved. The static values of the dielectric function's real component demonstrate a diminishing tendency with increasing photonic energy after a small and sharp increase. In all the studied phases, the

determined positive values of $\varepsilon_1(\omega)$ are a clear indication of conductive behavior, whereas negative values demonstrate the materials' insulating behavior. The static dielectric constants $\varepsilon_1(0)$ for the respective α , β , γ , and δ -phases of CdTe were computed (see Table 3) to be 6.1, 6.40, 6.41, and 8.10,

Table 3. Computed Zero Frequency Limits of Static Dielectric Constant $\varepsilon_1(0)$, Refractive Index $N(0)$, Reflectivity $R(0)$ for the Studied Structural Phases

	α -CdTe	β -CdTe	γ -CdTe	δ -CdTe	
$\varepsilon_1(0)$	6.1	6.40	6.41	8.10	this work
	6.8 ³⁵	6.46 ³⁵			other's work
	6.43 ³⁶				other's work
$n(0)$	2.41	2.55	2.55	2.58	this work
	2.52 ³⁵	2.56 ³⁵			other's work
	2.54 ³⁶				other's work
$R(0)$	0.17	0.19	0.19	0.27	this work
	0.21 ³⁵	0.20 ³⁵			other's work
	0.19 ³⁶				other's work

respectively. These $\varepsilon_1(0)$ values progressively decline because the energy band gap increases from phase to phase while going from the δ -phase toward the α -phase. For the α , β , γ , and δ -phases, the $\varepsilon_1(\omega)$ greatest peak position points are observed to exist at 2.9, 3.3, 2.6, and 2.2 eV accordingly, and the sharp peaks then steadily decline and get their minimum value in the range 5.0–7.0 eV. Furthermore, the real component of the dielectric function falls below the zero point, becoming negative at around 6.0, 3.9, 5.3, and 4.7 eV for the α - (cubic), β - (hexagonal), γ - (orthorhombic), and δ - (trigonal) phases, respectively, which is because of the incoming photon beam that is completely reflected from the media below the zero-point mark for the materials.

The imaginary component of the dielectric function $\varepsilon_2(\omega)$ is directly associated with material band gaps, and they are also determined for the α , β , γ , and δ -phases of the CdTe system, as illustrated in Figure 5b. In the $\varepsilon_2(\omega)$, the critical points are observed mostly in between the energy range of 2.0–4.0 eV in these phases. The optical change starts to occur at the 1.0–2.0 eV energy range. The energy values of the $\varepsilon_2(\omega)$ peaks of the CdTe material are at about 4.4, 3.2, 3.1, and 2.6 eV for the α , β , γ , and δ -phases of the CdTe system, respectively. In all these phases of the CdTe system, a decrease in $\varepsilon_2(\omega)$ is noticed when the energy values are increased. For each phase, the magnitude of the $\varepsilon_2(\omega)$ increases with energy above the threshold energy. Generally, the four phases exhibit similar dielectric functions over a wide energy range except for the δ - (trigonal) phases of the CdTe material. The results of the absorption coefficients in Figure 5c show that the absorption of photons starts at 1.5, 1.4, 1.2, and 1.1 eV for the α - (cubic), β - (hexagonal), γ - (orthorhombic), and δ - (trigonal) phases of the CdTe material, respectively. For an increase in the photon energies, the absorption coefficient increases for these phases and begins to reach the maximum peak values at approximately 4.7, 3.8, 3.95, and 4.8 eV for α , β , γ , and δ phases of the CdTe material, respectively. Some additional peaks (see Figure 5c) are also observed in the 2–6 eV energy range, which are due to the excitation of electrons from the valence band to the conduction band. The dynamic dielectric constant is used to calculate the energy loss function $L(\omega)$.

The plasma peak that describes the collective excitations of loosely bounded valence electrons into the unoccupied energy

levels of the conduction bands is a significant character of the $L(\omega)$ spectrum. As illustrated in Figure 5d the high intensity peaks in the $L(\omega)$ are detected at around 12.71, 12.60, 11.83, and 13.21 eV for the α - (cubic), β - (hexagonal), γ - (orthorhombic), and δ - (trigonal) phases of CdTe materials, respectively. Moreover, these high sharp peaks in the $L(\omega)$ then start to decrease along the energy axis, indicating plasma frequency. From these intense peaks of $L(\omega)$, we determined a decrease in these values that appear most commonly as rapid. This is most likely related to the predicted sharp peaks in the reflectivity and its crossing of the zero static value. The peak of the loss function corresponds to an abrupt type of reduction in the reflectivity spectrum $R(\omega)$. As seen in Figure 5e, the reflectivity spectra static values are observed at some low values of 0.17, 0.19, 0.19, and 0.27 for the α , β , γ , and δ -phases of CdTe, respectively. The $R(\omega)$ for the δ -phase is higher as compared to the other phases, and these high peaks arise from interband transition. Additionally, we also observed a sudden reduction in reflectivity spectra nearly at 8.0–9.0 eV energy range for all the α , β , γ , and δ -phases of the CdTe system that confirms the existence of collective plasma resonance. In the reflectivity profiles, the existence of a few high, sharp peaks located in the energy range of 3.0–10.0 eV for these phases of the CdTe material reveals that these phases are strong enough for high-frequency values and can be ideal protecting materials, specifically for large energy radiations.

The reflectivity then begins to upsurge linearly and rapidly at an energy value of about 13.5 eV in all these studied phases. As shown in Figure 5f, the refractive index static value $n(0)$ (see Table 3) was noticed at 2.41 for the α -phase, 2.55 for both the β - and γ -phases, and 2.58 for the δ -phase of the CdTe system. The refractive index rises as the incoming photon energy rise, with high peaks seen at energies of 2.90, 3.41, 3.34, and 2.20 eV for the α , β , γ , and δ -phases, respectively. The other peaks in the energy range of 3–6 eV are due to the interband transitions in these studied phases. The $n(0)$ values greater than one indicate that photons entering the compounds are slowed down by interactions with the electrons in the materials. Furthermore, for these $n(0)$ values, the phase velocity of light within the compounds is smaller than the speed of light in a vacuum. With increasing energy, the refractive index of each compound decreases, and the magnitude of $n(0)$ falls below one at high photon energies. Our findings show that the material band gap and the $n(\omega)$ are inversely related to one another in all the studied phases.

3.3. Thermoelectric Properties. We examined the thermoelectric behavior of the different phases of the CdTe system in its different phases, i.e., α - (cubic), β - (hexagonal), γ - (orthorhombic), and δ - (trigonal) and studied their respective thermoelectric features. We computed the relaxation time which is of utmost importance for the electronic transport coefficients of the potential thermoelectric materials and is based on the semi-classical Boltzmann transport theory. The computed τ_p (fs) values were 183 fs, 174 fs, 171 fs, and 169 fs for α - (cubic), β - (hexagonal), γ - (orthorhombic), and δ - (trigonal) studied structural phases. Figure 6a–d explains the thermal conductivity, Seebeck coefficient, specific heat capacity, and figure of merit for these phases. In the case of semiconductors, the lattice vibrations associated with the number of atoms increase as the temperature rises. Convection is capable of moving heat from a higher potential region to a low potential region. Additionally, thermal conductivity for the semiconductors in most cases is probably administered by the

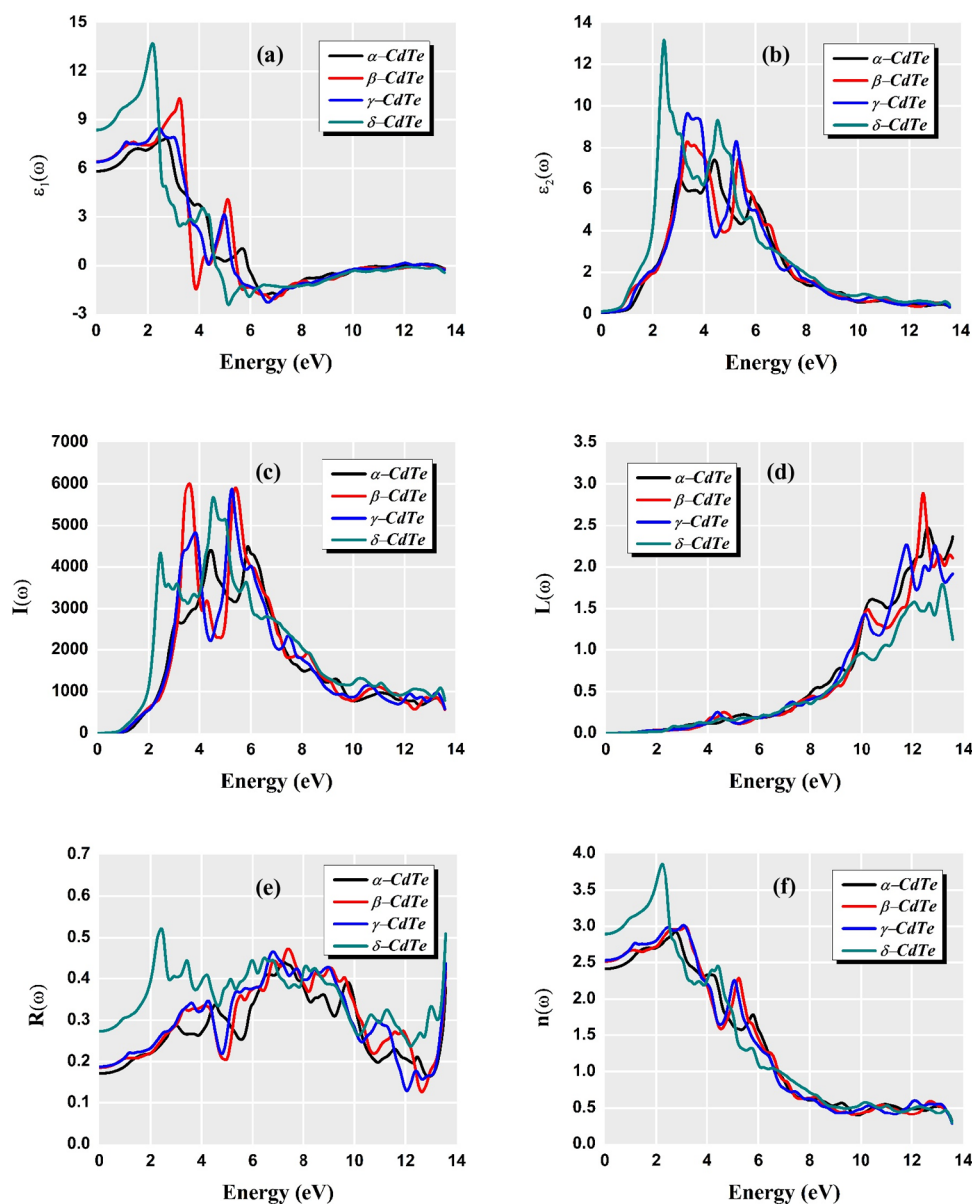


Figure 5. Computed (a) real part $\varepsilon_1(\omega)$ and (b) imaginary part $\varepsilon_2(\omega)$ of the dielectric function, (c) absorption coefficient $I(\omega)$, (d) electron energy loss function $L(\omega)$, (e) reflectivity spectra $R(\omega)$, and (f) refractive index $n(\omega)$ for the four different structural phases of the CdTe system.

involvement of phonons and electrons. The thermal conductivity (κ) displays the tendency of a material to conduct heat. We measured the electrical part of thermal conductivity (κ_e). Heat is not only carried by free electrons in metals but also by lattice vibrations phonons in semiconductors and insulators. Thermal conductivity exhibits a similar increasing trend as electrical conductivity. The graphs indicate that thermal conductivity rises approximately equally from negative to positive values through the temperature range from 100 to 850 K due to the charge carrier's thermal excitation, and this enhances the process of heat conduction. At 100 K temperature, the values of thermal conductivity were found to be 0.5×10^{15} W/mK, 0.48×10^{15} W/mK, 0.37×10^{15} W/mK, 0.23×10^{15} W/mK for (α , β , γ , and δ) phases of the CdTe material, respectively. Consequently, at 300 K, the κ values are about 1.3×10^{15} W/mK, 1.3×10^{15} W/mK, 1.26×10^{15} W/mK, and 0.6×10^{15} W/mK for the α , β , γ , and δ phases, respectively. For an increase in temperature up to a value of 850 K, the thermal conductivity attains values of about $3.58 \times$

10^{15} W/mK, 3.43×10^{15} W/mK, 3.21×10^{15} W/mK, and 3.21×10^{15} W/mK for these four α , β , γ , and δ phases, respectively. From the shown plots, the α , β , and γ phases have a higher thermal conductivity than the δ -phase, this trend in " κ " could make the α , β , and γ phases of the CdTe system as potential thermoelectric materials at extreme temperatures.

The Seebeck coefficient is also crucial in understanding the material efficiency in terms of their thermoelectric applications. The Seebeck coefficient, as calculated for the (α , β , γ , and δ) phases, of the CdTe system is plotted with temperature. The Seebeck coefficient of the α -cubic phase is substantially greater than those of the γ and δ phases of the material above 300 K and possesses the same value as that of the β -phase below 300 K, as can be seen in Figure 6b. In the α -phase, at 100 K, the Seebeck coefficient begins at a lower value of $0.0 \mu\text{V K}^{-1}$ and then rises as the temperature goes up and reaches a value of $8.45 \mu\text{V K}^{-1}$ at 850 K. However, for the β , γ , and δ phases of the CdTe system, the Seebeck coefficient starts with a negative value of -1.1 , -0.2 , and $-1.6 \mu\text{V K}^{-1}$ at a temperature of 100

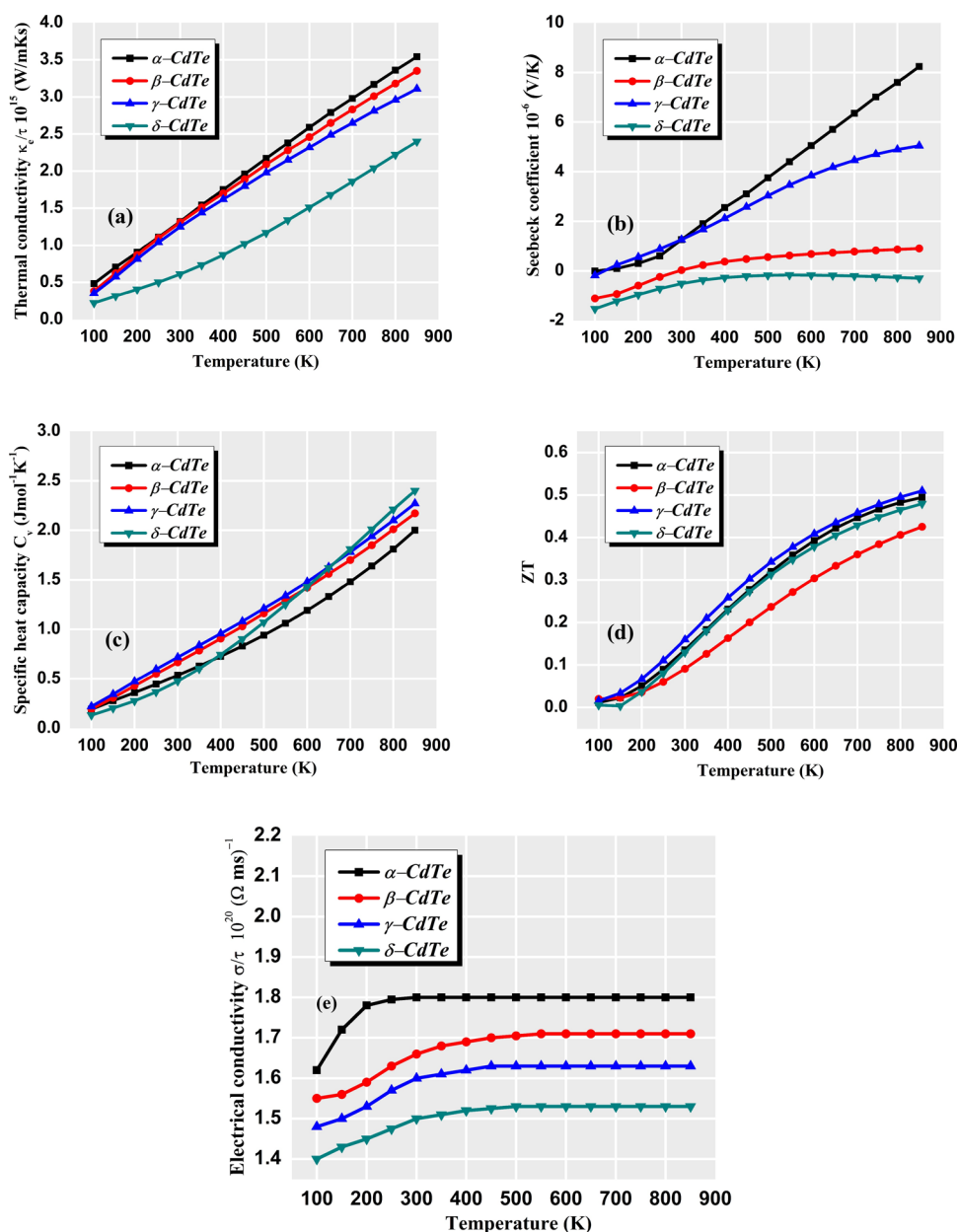


Figure 6. Computed temperature-dependent (a) thermal conductivity, (b) Seebeck coefficient, (c) specific heat capacity, (d) figure of merit, and (e) electrical conductivity, for the four different structural phases of the CdTe system.

K and the value for the case of the γ -phase then rapidly rises to a value of $5.0 \mu\text{V K}^{-1}$ at 850 K. At 100 K, the Seebeck coefficient for the β -ZnSe (hexagonal) begins with a negative value of $-1.1 \mu\text{V K}^{-1}$. The value of the β -phase approaches $0.0 \mu\text{V K}^{-1}$ at 300 K, and the value rises as the temperature increases, reaching a value of $1.0 \mu\text{V K}^{-1}$ at 850 K. The Seebeck coefficient values in the positive region indicate the existence of the dominant charge carrier in the given temperature range. A negative Seebeck value means that electrons are the dominant conductors in these materials.

An alternative understanding concerning the lattice vibrations is achieved through specific heat capacity (C_v). The investigated specific heat capacity (C_v) as a function of temperature is presented in Figure 6c, which reveals that at higher temperature values, the γ - and δ -phases possess a larger C_v value as compared to α - and β -phases. With a rise in temperature, the C_v value of these materials rises. We analyzed

specific heat capacity only on the basis of electronic contributions. At a lower temperature of 100 K, the calculated specific heat capacity values of the α , β , γ , and δ -phases are 0.21, 0.20, 0.23, and 0.15 $\text{J mol}^{-1} \text{K}^{-1}$, respectively. We noticed the C_v values at 300 K to be 0.71 and 0.74 for the β and γ -phases, and 0.5, and 0.12 $\text{J mol}^{-1} \text{K}^{-1}$ for the α and δ -phases, respectively. The high temperature value of C_v approaches 3.59, 3.48 $\text{J mol}^{-1} \text{K}^{-1}$ and 3.21, 2.45 $\text{J mol}^{-1} \text{K}^{-1}$ for the α , β , γ , and δ phases at 850 K, respectively. As a result, materials with less specific heat capacity can recognize and show temperature variations efficiently, which is the case for the δ phases. Materials having a high specific heat capacity, on the other hand, are appropriate for constructing oven covers and insulating materials; this nature was concluded in the α and β -phases. Another transport parameter that is used to examine the material proficiency is the figure of merit (ZT). To evaluate the effectiveness of thermoelectric nature in these studied

phases, the dimensionless figure of merit (ZT) is computed and is expressed as follows:^{41,42}

$$ZT = \frac{S^2 \sigma}{\kappa_1 + \kappa_e} T \quad (9)$$

The variation in the figure of merit with the temperature is analyzed, as shown in Figure 6d; the figure of merit (ZT) is calculated up to a temperature value of 850 K for the α , β , γ , and δ -phases of the CdTe system, as shown in Figure 6d. At about 100 K, the ZT was noticed to be 0.01, 0.02, 0.01, and 0.009 for α -, β -, γ -, and δ -phases, respectively. The ZT values of the γ -phase are higher compared to the other three phases with the increase in temperature. At 300 K, the ZT values for α -, β -, γ -, and δ -phases are 0.13, 0.09, 0.17, and 0.13, respectively. At 850 K, a maximum value of ZT was observed that approached 0.49 for the α phase, 0.42 for the β phase, 0.51 for the γ phase, and 0.48 for δ phase, respectively. Similarly, from 100 to 850 K, these computed ZT plots display a similar trend with a small variation in their values. The γ -phase displays an exceptional value in between both temperature ends, suggesting it to be the ideal thermoelectric material in this range. The ZT value for the β -phases is much lesser, concluding that it is not much appropriate for thermoelectric applications in its pure form at very low and high temperatures. Figure 6e shows the computed electric conductivity for the studied phases of the CdTe system. The plots show a slight increase up to room temperature in all these structural phases due to the rise in the carrier concentration in these studied phases. The α -phase displays a better electrical conductivity as compared to the other phases. At 300 K temperature, the electrical conductivity for the studied phases were $1.80 \times 10^{20} (\Omega \text{ ms})^{-1}$, $1.66 \times 10^{20} (\Omega \text{ ms})^{-1}$, and $1.60 \times 10^{20} (\Omega \text{ ms})^{-1}$, and $1.50 \times 10^{20} (\Omega \text{ ms})^{-1}$ for the α -, β -, γ -, and δ -phases, respectively. Beyond the temperature value of 450 K, the electrical conductivity for all the studied phases gives a linear nature with a constant value up to a temperature of 850 K.

4. CONCLUSIONS

In summary, the optoelectronic and thermoelectric properties of the four different structural phases for the CdTe material were computed with state-of-the-art DFT calculations. The mBJLDA pseudopotential plane-waves calculations were performed to get the gap values of 1.45, 1.49, 1.48, and 0.75 eV for the cubic, hexagonal, orthorhombic, and trigonal phases respectively. The studied phases display a direct band gap nature for the α -cubic, β -hexagonal, γ -orthorhombic, and an indirect band type nature for the δ -trigonal phase from the A-point at the valence band maxima to the Γ -point at the conduction band minima. The PDOS show that for all structures, the upper valence bands are mainly formed by the anion Te p -states, while the lower conduction band has the cation Cd s -character, with the Cd bands of the p -character appearing higher in energy in the conduction region. From the PDOS plots, the main valence band width in the trigonal δ -CdTe is larger than that in the other structures, indicating very less localization of the Te p -bands. The optical change in the imaginary component occurs at the 1.0 to 2.0 eV energy range. The $\varepsilon_2(\omega)$ increases with energy above the threshold energy. These structural phases exhibit similar dielectric functions over a wide energy range except the δ - (trigonal) phases of the CdTe material. The absorption of photons starts at around 1.5, 1.4, 1.2, and 1.1 eV for α - (cubic), β - (hexagonal), γ - (orthorhom-

bic), and δ - (trigonal) phases, respectively. Some intense sharp peaks in the $L(\omega)$ start to decrease along the energy axis indicating plasma frequency. Similarly, a sudden reduction in reflectivity spectra nearly at around 9.0 eV energy range in all the structural phases of the system confirms the existence of collective plasma resonance. The thermal conductivity rises approximately equally from negative to positive values due to the charge carrier's thermal excitation; this enhances the heat process of conduction. From the computed plots, the α , β , and γ phases have higher thermal conductivity than the δ -phase, and this mounting trend makes the α , β , and γ phases of the CdTe system as potential thermoelectric materials at extreme temperatures. The Seebeck coefficient of the α -cubic phase is noticed to be greater than those of the γ and δ phases and has a same value as that of the β -phase at around 300 K. The ZT values of the γ -phase show an increasing trend as compared to the other three phases with the increase in temperature. The γ -phase displays an exceptional value in between both temperature ends, suggesting it to be an ideal thermoelectric material in this range.

AUTHOR INFORMATION

Corresponding Author

Muhammad Salman Khan – Department of Physics, Abdul Wali Khan University, Mardan 23200, Pakistan;
orcid.org/0000-0001-9909-0883;
Email: salmankhan73030@gmail.com

Authors

Hazem Abu-Farsakh – Department of Mathematics and Sciences, Prince Sultan University, Riyadh 11586, Saudi Arabia

Banat Gul – National University of Sciences and Technology (NUST), Islamabad 24090, Pakistan

Complete contact information is available at:

<https://pubs.acs.org/10.1021/acsomega.3c00757>

Notes

The authors declare no competing financial interest.

ACKNOWLEDGMENTS

The first author would like to thank Prince Sultan University for their support.

REFERENCES

- (1) Knoesel, E.; Bonn, M.; Shan, J.; Heinz, T. F. Charge Transport and Carrier Dynamics in Liquids Probed by Thz Time-Domain Spectroscopy. *Phys. Rev. Lett.* **2001**, *86*, 340–343.
- (2) Contreras-Puente, G.; Vigil, O.; Ortega-López, M.; Morales-Acevedo, A.; Vidal, J.; Albor-Aguilera, M. L. New Window Materials Used as Heterojunction Partners on CdTe Solar Cells. *Thin Solid Film.* **2000**, *361–362*, 378–382.
- (3) Schall, M.; Walther, M.; Uhd Jepsen, P. Fundamental and Second-Order Phonon Processes in CdTe and ZnTe. *Phys. Rev. B* **2001**, *64*, No. 094301.
- (4) Contreras-Puente, G.; Vigil, O.; Ortega-López, M.; Morales-Acevedo, A.; Vidal, J.; Albor-Aguilera, M. L. New Window Materials Used as Heterojunction Partners on CdTe Solar Cells. *Thin Solid Film.* **2000**, *361–362*, 378–382.
- (5) Khan, M. S.; Gul, B.; Khan, G.; Benaadad, M.; Ghlamallah, B.; Ali Khattak, S.; Khan, T.; Zulfikar, S.; Shah, S. K.; Adil Khan, M. Ab-Initio Study about the Electronic, Optical and Thermoelectric Nature of α -, β -, and γ -Phases of CdS Semiconductor: Using the Accurate M-BJ Approach. *Phys. Scr.* **2021**, *96*, No. 055803.

- (6) Merad, A. E.; Aourag, H.; Khelifa, B.; Mathieu, C.; Merad, G. Predictions of the Bonding Properties INCD1–XZnxTe. *Superlattices Microstruct.* **2001**, *30*, 241–251.
- (7) Kanoun, M. B.; Merad, A. E.; Aourag, H.; Cibert, J.; Merad, G. Molecular-Dynamics Simulations of Structural and Thermodynamic Properties of ZnTe Using a Three-Body Potential. *Solid State Sci.* **2003**, *5*, 1211–1216.
- (8) Wei, S.-H.; Zhang, S. B.; Zunger, A. First-Principles Calculation of Band Offsets, Optical Bowings, and Defects in Cds, CdSe, CdTe, and Their Alloys. *J. Appl. Phys.* **2000**, *87*, 1304–1311.
- (9) Khan, M. S.; Gul, B.; Khan, G.; Ghulamallah, B.; Khattak, S. A.; Khan, M.; Khan, T.; Ajaz, M.; Zulfiqar, S.; Muhammad, W. Insight into the Electronic, Optical and Transport Nature of Al₂CdX₄ (X = S, Se and Te) Employing the Accurate mBJ Approach: Novel Materials for Opto-Electronic Devices. *Mater. Sci. Semicond. Process.* **2021**, *135*, No. 106098.
- (10) Marple, D. T. Effective Electron Mass in CdTe. *Phys. Rev.* **1963**, *129*, 2466–2470.
- (11) Ambrosch-Draxl, C.; Sofo, J. O. Linear Optical Properties of Solids within the Full-Potential Linearized Augmented Plane-wave Method. *Comput. Phys. Commun.* **2006**, *175*, 1–14.
- (12) Pandey, S. K.; Tiwari, U.; Raman, R.; Prakash, C.; Krishna, V.; Dutta, V.; Zimik, K. Growth of Cubic and Hexagonal CdTe Thin Films by Pulsed Laser Deposition. *Thin Solid Film.* **2005**, *473*, 54–57.
- (13) Merad, A. E.; Kanoun, M. B.; Merad, G.; Cibert, J.; Aourag, H. Full-Potential Investigation of the Electronic and Optical Properties of Stressed CdTe and ZnTe. *Mater. Chem. Phys.* **2005**, *92*, 333–339.
- (14) Huang, M.-Z.; Ching, W. Y. Calculation of Optical Excitations in Cubic Semiconductors. I. Electronic Structure and Linear Response. *Phys. Rev. B* **1993**, *47*, 9449–9463.
- (15) Deligoz, E.; Colakoglu, K.; Ciftci, Y. Elastic, Electronic, and Lattice Dynamical Properties of CdS, CdSe, and CdTe. *Phys. B* **2006**, *373*, 124–130.
- (16) Dubowski, J. J.; Thompson, J. R.; Rolfe, S. J.; McCaffrey, J. P. Laser Induced Growth of Cd_{1-x}MnxTe and CdTeCd_{1-x}MnxTe. *Superlattices Microstruct.* **1991**, *9*, 327–330.
- (17) Markowski, R.; Podgorny, M. Optical Absorption in CdTe: D-Core Transitions. *J. Condens. Matter Phys.* **1991**, *3*, 9041–9053.
- (18) Alouani, M.; Brey, L.; Christensen, N. E. Calculated Optical Properties of Semiconductors. *Phys. Rev. B* **1988**, *37*, 1167–1179.
- (19) Cardona, M.; Greenaway, D. L. Fundamental Reflectivity and Band Structure of ZnTe, CdTe, and HGTE. *Phys. Rev.* **1963**, *131*, 98–103.
- (20) Davis, P. W.; Shilliday, T. S. Some Optical Properties of Cadmium Telluride. *Phys. Rev.* **1960**, *118*, 1020–1022.
- (21) Gonze, X.; Amadon, B.; Antonius, G.; Arnardi, F.; Baguet, L.; Beuken, J.-M.; Bieder, J.; Bottin, F.; Bouchet, J.; Bousquet, E.; et al. The Abinitproject: Impact, Environment and Recent Developments. *Comput. Phys. Commun.* **2020**, *248*, No. 107042.
- (22) Romero, A. H.; Allan, D. C.; Amadon, B.; Antonius, G.; Applencourt, T.; Baguet, L.; Bieder, J.; Bottin, F.; Bouchet, J.; Bousquet, E.; et al. Abinit: Overview and Focus on Selected Capabilities. *J. Chem. Phys.* **2020**, *152*, No. 124102.
- (23) Hamann, D. R. Erratum: Optimized Norm-Conserving Vanderbilt Pseudopotentials. *Phys. Rev. B* **2017**, *95*, No. 239906.
- (24) (a) Abu-Farsakh, H.; Abu-Jafar, M.; Qteish, A. Modified Becke-Johnson Calculations Using Norm-Conserving Pseudopotential Plane-Wave Approach: Systematic Analysis. *Mater. Today Commun.* **2021**, *26*, No. 101748. (b) Perdew, J. P.; Burke, K.; Ernzerhof, M. Generalized Gradient Approximation Made Simple. *Phys. Rev. Lett.* **1996**, *77*, 3865–3868.
- (25) Schwarz, K.; Blaha, P.; Madsen, G. K. H. Electronic Structure Calculations of Solids Using the WIEN2K Package for Material Sciences. *Comput. Phys. Commun.* **2002**, *147*, 71–76.
- (26) Tran, F.; Blaha, P. Accurate Band Gaps of Semiconductors and Insulators with a Semi local Exchange-Correlation Potential. *Phys. Rev. Lett.* **2009**, *102*, No. 226401.
- (27) Barnes, B. Optical Properties of Solids, 2nd EDN, by Mark Fox. *Contemp. Phys.* **2011**, *52*, 612–613.
- (28) Wooten, F. *Optical Properties of Solids*, Academic Press, Inc.: Cambridge, Massachusetts, 2013.
- (29) Wang, H.; Wang, Y.; Cao, X.; Zhang, L.; Feng, M.; Lan, G. Simulation of Electronic Density of States and Optical Properties of PbB₄O₇ by First-Principles DFT Method. *Phys. Status Solidi B* **2009**, *246*, 437–443.
- (30) Perdew, J. P.; Burke, K.; Ernzerhof, M. Generalized Gradient Approximation Made Simple. *Phys. Rev. Lett.* **1996**, *77*, 3865–3868.
- (31) Tran, F.; Blaha, P. Accurate Band Gaps of Semiconductors and Insulators with a Semilocal Exchange-Correlation Potential. *Phys. Rev. Lett.* **2009**, *102*, No. 226401.
- (32) Tran, F.; Doumont, J.; Kalantari, L.; Huran, A. W.; Marques, M. A.; Blaha, P. Semilocal Exchange-Correlation Potentials for Solid-State Calculations: Current Status and Future Directions. *J. Appl. Phys.* **2019**, *126*, No. 110902.
- (33) Abu-Farsakh, H.; Qteish, A. Performance of the Modified Becke–Johnson Potential Employing the Pseudopotential Plane-Wave Approach for Band Structure Calculations. *Comput. Mater. Sci.* **2022**, *208*, No. 111324.
- (34) Mei, J. R.; Lemos, V. Photoluminescence on CdSe and CdTe under Hydrostatic Pressure. *Solid State Commun.* **1984**, *52*, 785–788.
- (35) Hosseini, S. M. Optical Properties of Cadmium Telluride in Zinc-Blende and Wurtzite Structure. *Phys. B* **2008**, *403*, 1907–1915.
- (36) Zhang, C.; Sa, R.; Liu, D. The Influence of Minor MG Doping on the Physical Properties of CdTe: A DFT Study. *J. Chem. Phys.* **2022**, *562*, No. 111674.
- (37) Khan, M. S.; Gul, B.; Abu-Farsakh, H.; Khan, G. Insight into the Optoelectronic and Thermoelectric Nature of NaLiX (X = S, Se, Te) Novel Direct Bandgap Semiconductors: A First-Principles Study. *J. Mater. Chem. C* **2022**, *10*, 12001–12011.
- (38) Jain, A.; Ong, S. P.; Hautier, G.; Chen, W.; Richards, W. D.; Dacek, S.; Cholia, S.; Gunter, D.; Skinner, D.; Ceder, G.; et al. Commentary: The Materials Project: A Materials Genome Approach to Accelerating Materials Innovation. *APL Mater.* **2013**, *1*, No. 011002.
- (39) Khan, M. S.; Gul, B.; Ahmad, B.; Khan, G.; Khattak, S.; Khan, T.; Ajaz, M.; Zulfiqar, S.; Wahab, F. Investigating the Optoelectronic and Thermoelectric Nature of IrSbX (X = S, Se, And Te) TMC's Semiconductors: By Employing the Accurate Modified Becke-Johnson Exchange Potential. *Mater. Sci. Semicond. Process.* **2022**, *144*, No. 106577.
- (40) Kumar, M.; Singh, A.; Gill, D.; Bhattacharya, S. Optoelectronic Properties of Chalcogenide Perovskites by Many-Body Perturbation Theory. *J. Phys. Chem. Lett.* **2021**, *12*, 5301–5307.
- (41) Thanh, V. V.; Truong, D. V.; Tuan Hung, N. Janus γ -Gesse Monolayer as a High-Performance Material for Photocatalysis and Thermoelectricity. *ACS Appl. Energy Mater.* **2023**, *6*, 910–919.
- (42) Hung, N. T.; Nugraha, A. R.; Yang, T.; Zhang, Z.; Saito, R. Thermoelectric Performance of Monolayer InSe Improved by Convergence of Multivalley Bands. *J. Appl. Phys.* **2019**, *125*, No. 082502.